Friction **12**(3): 554–568 (2024)
https://doi.org/10.1007/s40544-023-0795-x
ISSN 2223-7690
CN 10-1237/TH

RESEARCH ARTICLE

Finite element analysis and experimental validation of polymer–metal contacts in block-on-ring configuration

K. Y. Eayal AWWAD[1,*], Khosro FALLAHNEZHAD[2], B. F. YOUSIF[3], Ahmad MOSTAFA[1], Omar ALAJARMEH[3], A. SHALWAN[4], Xuesen ZENG[3]

[1] *Mechanical Engineering Department, Faculty of Engineering, Tafila Technical University, Tafila 66110, Jordan*

[2] *Medical Device Research Institute, College of Science and Engineering, Flinders University, South Australia 5042, Australia*

[3] *Centre for Future Materials, University of Southern Queensland, Toowoomba 4350, Australia*

[4] *Department of Manufacturing Engineering Technology, Public Authority for Applied Education and Training, Kuwait 13092, Kuwait*

Received: 21 March 2023 / Revised: 22 May 2023 / Accepted: 02 July 2023

Abstract: The wear profile analysis, obtained by different tribometers, is essential to characterise the wear mechanisms. However, most of the available methods did not take the stress distribution over the wear profile in consideration, which causes inaccurate analysis. In this study, the wear profile of polymer–metal contact, obtained by block-on-ring configuration under dry sliding conditions, was analysed using finite element modelling (FEM) and experimental investigation. Archard's wear equation was integrated into a developed FORTRAN–UMESHMOTION code linked with Abaqus software. A varying wear coefficient (k) values covering both running-in and steady state regions, and a range of applied loads involving both mild and severe wear regions were measured and implemented in the FEM. The FEM was in good agreement with the experiments. The model reproduced the stress distribution profiles under variable testing conditions, while their values were affected by the sliding direction and maximum wear depth (h_{max}). The largest area of the wear profile, exposed to the average contact stresses, is defined as the normal zone. Whereas the critical zones were characterized by high stress concentrations reaching up to 10 times of that at the normal zone. The wear profile was mapped to identify the critical zone where the stress concentration is the key point in this definition. The surface features were examined in different regions using scanning electron microscope (SEM). Ultimately, SEM analysis showed severer damage features in the critical zone than that in the normal zone as proven by FEM. However, the literature data presented and considered the wear features the same at any point of the wear profile. In this study, the normal zone was determined at a stress value of about 0.5 MPa, whereas the critical zone was at about 5.5 MPa. The wear behaviour of these two zones showed totally different features from one another.

Keywords: polymer-to-metal contact; block-on-ring; wear profile; wear model

1 Introduction

Wear is an essential factor affecting the reliability of mechanical components and thus, it influences their service life [1–3]. The wear phenomenon occurs in different forms, such as sliding, erosive, fretting, adhesive, abrasive, and chemical. Sliding wear is considered the most common type and mechanically the most complex form [2, 4]. Often, experimental testing techniques like pin-on-drum, pin-on-disc (POD), linear tribo-machine, and block-on-ring (BOR) are used to determine the wear performance of various materials before implementing them in real tribological applications. These experimental techniques are configured in such a way to mimic the actual contact of tribosystems considering the main affecting parameters,

* Corresponding author: K. Y. Eayal AWWAD, E-mail: K.awwad@ttu.edu.jo

such as sliding velocity, applied pressure, and sliding distance, etc. The BOR configuration tries to imitate the circumferential contact experienced by a wide range of tribo-components, such as bearings, bushings, gears, camshafts, and so on [5]. Such experiments provide a qualitative study for the proposed materials used in a specific application. However, the geometrical effect and localised stress fields of such configurations are experimentally indeterminate. Therefore, modelling of these wear experiments is essential to provide quantitative data on the localised stresses, which describes the wear process in-depth.

In order to evaluate the wear phenomenon, many governing equations have been derived over the past few decades. In their comprehensive and in-depth review on wear equations, Meng and Ludema [6] stated that there are more than 300 wear modelling equations, which can be sorted into three different approaches. First, empirical equations, which are directly formed based on experimental data under varying wear conditions. Typically, this approach shows precise results, but it is only valid for a very specific range of test parameters. Second, equations can be formed depending on material failure mechanisms, in which the mechanical properties, such as fracture toughness, material flow, and fracture strain, etc., are included. However, due to the long derivations and complexity of this kind of equations, no equations were reproduced [6]. Third, contact mechanics-based models, which simplify the relationship between the working parameters. One of the most famous wear equations in this model is Archard's wear equation [7]. Archard's equation takes into account the abrasive and adhesive wear mechanisms assuming that the wear volume (V) is directly proportional to the load (F) and the sliding distance (S); while inversely proportional to the yield stress or the hardness (H) of the softer surface. The proportionality constant of this relationship is defined as the wear coefficient (k) of the material.

$$\frac{V}{S} = k\frac{F}{H} \tag{1}$$

Many attempts have been made to modify this equation to meet the requirements of specific cases. For instance, according to Bradford [8], Sarkar [9] has modified Archard's model so that coefficient of friction (COF) was calculated and its value was related to the volume of worn material. Another example is related to the wear of highly elastic/pseudo-elastic materials [10]. Archard's wear equation gives a simple model for the wear mechanism and has the flexibility to comply with specific cases of the wear process and for variant material properties.

In the recent decade, many researchers [3, 11–14] have used the finite element method (FEM) to simulate different types of wear forms. This method in fact can be used to predict and enrich the understanding of such physical phenomenon. A wear simulation tool (wear processor), developed by Hegadekatte et al. [15], has been used to simulate the deformable-to-deformable contact problem in two-dimensions (2D) and 3D modes. Despite the good accuracy of the model, when compared to the experiments, the model can only be used for low applied loads until 400 mN. In fact, 800 mN showed a significant inconsistency with experiments. More recently, a limited number of studies about sliding wear modelling were developed based on an adaptive FEM. By using this tool, the grid of the mesh can be highly controlled, which provides more accurate results for the wear process analysis [12, 16, 17].

Simulating the wear process for different types of tribometers is essential as it gives the opportunity to validate the outcomes by the experiments. The POD tribometer, which is the most frequently mentioned in the literature, has been widely studied and modelled for different types of materials, including both cases of metal-to-metal contact [11, 12] and polymer-to-metal contact [18]. Moreover, experimental findings were widely used as simulation-input data for variant tribological applications [3, 11, 12, 14]. Martinez et al. [14] simulated the dry sliding wear in a POD configuration for a polymer-to-metal contact pair based on Archard's model, where the pin had a flat-surface end. However, it was reported that wear is highly sensitive to the stress concentration regions as well as to the high COF values. In another study, Bortoleto et al. [11] simulated the unlubricated sliding wear of metal-to-metal contact in the configuration of 3D POD. The model was developed using Abaqus linked with the UMESHMOTION subroutine, based on Archard's model. The results showed high accuracy

as compared to experimental outcomes, and it was reported that the model has a high capability to predict the transition wear region. However, the stress was distributed over the worn surface in an unclear pattern, which is attributed to the nature of POD contact configuration. Other tribometer configurations showed that the stress distribution over the wear profile have uniform patterns. For instance, Yue and Abdel Wahab [19] developed a 2D fretting wear model to simulate a contact pair of cylindrical pad and a flat specimen. According to these authors, contact pressure distribution for different layer thicknesses along with a variant number of cycles showed a consistent stress distribution pattern over the wear profile. The stress concentration exhibited a uniform distribution at both edges of the wear profile, which mainly attributed to the oscillatory motion at the contact interface. Similar stress distribution profiles were observed in Refs. [20, 21].

In polymer tribology, it is expected that the geometrical changes are high, as it is well known that polymers are more deformable compared to metals. Thus, in this kind of material, the geometrical change under the wear progress may have a major impact on the wear process. In polymer–metal contact, polymers sacrifice for the tribosystem by creating a transfer film on the metallic counterpart. Experientially, in POD configuration, the contact area is constant with wear progress, because of the flat-on-flat contact between the pin and the disc. On the contrary, a BOR configuration mimics the real contact of a wide range of tribo-components more closely in which the contact of tribo-system is circumferential, such as rubber tyres, camshafts, bushings, pulleys, and bearings [5]. The variable geometry of BOR configuration along with the progressive wear process may exert a direct impact on the distribution of the stress concentration on the worn surfaces.

This work aims at developing a unique adaptive finite element (FE) model to simulate the dry adhesive wear mechanism of a polymer–metal contact pair in BOR configuration. Accordingly, the effect of the progressive wear process on the stress distribution over the wear profile was investigated. The wear parameters were chosen to cover both mild and severe regions as well as both running-in and steady state regions. Furthermore, the surfaces of the experimentally tested specimens were examined using scanning electrons microscope (SEM). The experimental results were compared with the wear profile data extracted by the FE analysis to validate the model.

2 Methodology

2.1 Materials characteristics

The main raw material utilised to prepare the tensile and wear specimens was epoxy resin (R246TX) along with the (H160) curing hardener. These materials were provided by ATL Composites Pty., Ltd., Australia. Epoxy resin was selected due to its widely usage as a base matrix for polymer composites under wear conditions [22–24]. It is also used in composite forms as a load-bearing material, such as composite brakes in automobiles [25]. Tensile tests were conducted in conformity with ASTM D638-14 standard test [26]. A hardness tester, with a durometer Type D, was used to measure the shore D hardness of the specimens, in conformity with ASTM D2240 standard test [27]. For repeatability and reproducibility of the results, three tensile specimens were tested, and for the hardness test, three readings were taken for each sample. Both average and standard deviation values were calculated for the tensile and hardness results. The mechanical properties of the epoxy, taken from the work of Eayal Awwad et al. [23], are presented in Table 1.

The dry adhesive wear test of epoxy was conducted on a BOR tribometer, following the ASTM G77-17 standard test [28] using the listed parameters in Table 2. The wear specimens were slid against a 228 mm diameter and 20 mm thick AISI 304 stainless steel disc (counterface), shown in Fig. 1(a), of 150 HB hardness. The sacrificing blocks of 58 mm × 25 mm × 20 mm (length × width × thickness), as illustrated in Fig. 1(b), were made from epoxy. The configuration of the wear test system using BOR tribometer is described in Fig. 1(c). The roughness, *R*a values, were

Table 1 The mechanical properties of epoxy [23].

Ultimate tensile strength (MPa)	61.5 ± 3.3
Stiffness (GPa)	1.16 ± 0.04
Fracture strain (%)	7.9 ± 1.5
Shore D hardness	79.0 ± 0.82

Table 2 Dry adhesive wear test parameters.

Test specimen		
	Ring	Stainless steel AISI 304 (Ø228 mm × 20 mm)
	Block	Epoxy (58 mm × 25 mm × 20 mm)
Sliding distance		6 km
Sliding speed		2 m/s
Applied load		15, 30, 45, and 60 N
Pressure velocity		0.33–3.9 MPa·m·s^{-1}
Test temperature		~20 °C

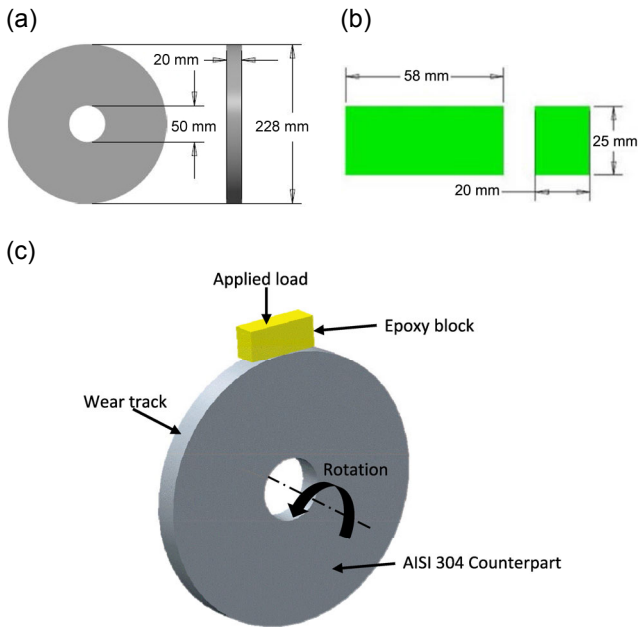

Fig. 1 Schematic drawings of (a) the AISI 304 stainless steel ring, (b) the adhesive wear specimens, and (c) a schematic illustration of BOR test configuration.

controlled to be less than *R*a = 0.2 μm for the epoxy and steel counterface, prior the test, by polishing both surfaces according to the experimental procedure reported in [23].

The adhesive wear tests were carried out for 6 km of sliding distance and under different pressure velocity (*PV*) values. The sliding distance was selected to reach the steady state region of the wear process. The pressure values were determined based on the calculated contact area by using FEM. The sliding speed was fixed at 2 m/s for all tests while the applied load ranged from 15 to 60 N. These values were selected to cover both mild and severe wear regions, where *PV* fluctuates between 0.33 and 3.9 MPa·m·s^{-1} [23, 24]. The tests were carried out at room temperature ~20 °C. A Mettler Toledo load cell monitor with an accuracy of 0.0098 N was used to calculate the COF. The mass loss was obtained using a mass scale with an accuracy of 1×10^{-5} g. Figure 2(a) illustrates the geometry of the worn volume. The volume was measured based on the mass loss. The maximum wear depth of the wear profile was assessed based on the wear profile, shown in Fig. 2(b), obtained by a surface roughness tester. The maximum wear depth was substituted in Eq. (2) to find the worn volume [29]:

$$V(R, W, h) = W\left[R^2\cos^{-1}\left(\frac{R-h}{R}\right)-(R-h)\sqrt{2Rh-h^2}\right] \tag{2}$$

where V is the volume of the worn material (mm^3), W is the length of the wear scar, R is the radius of the ring (mm), and h is the wear depth (mm). The wear coefficient k was calculated based on Eq. (3) [30]:

$$k = \frac{\Delta V}{LF_N}\ (\text{mm}^3/(\text{N}\cdot\text{mm})) \tag{3}$$

where ΔV is the worn volume (mm^3), L is the sliding distance (m), and F_N is the normal load (N). Both average and standard deviation values of k and COF were calculated based on the minimum number of attempts recommended by the ASTM G77 standard [28].

Table 3 shows the adhesive wear characteristics of the epoxy, including k and COF as average values, over 6 km of sliding distance. The epoxy specimens were tested under four cases of applied load (15, 30, 45, and 60 N). k values were calculated after every 1 km of sliding distance while the COF values were obtained for every case over the entire length of sliding distance, i.e., 6 km.

A JEOL-Smart Coater was used to improve the electrical conductivity on the surfaces of the test specimens by sputtering a very thin gold layer. The topography of the worn surfaces was examined by using a Benchtop SEM MODEL JCM-6000 at 5 KV accelerating voltage. The features of the examined surfaces were then used to analyse the wear profile in each region.

2.2 Numerical modelling

FEM was used to simulate the adhesive wear form of

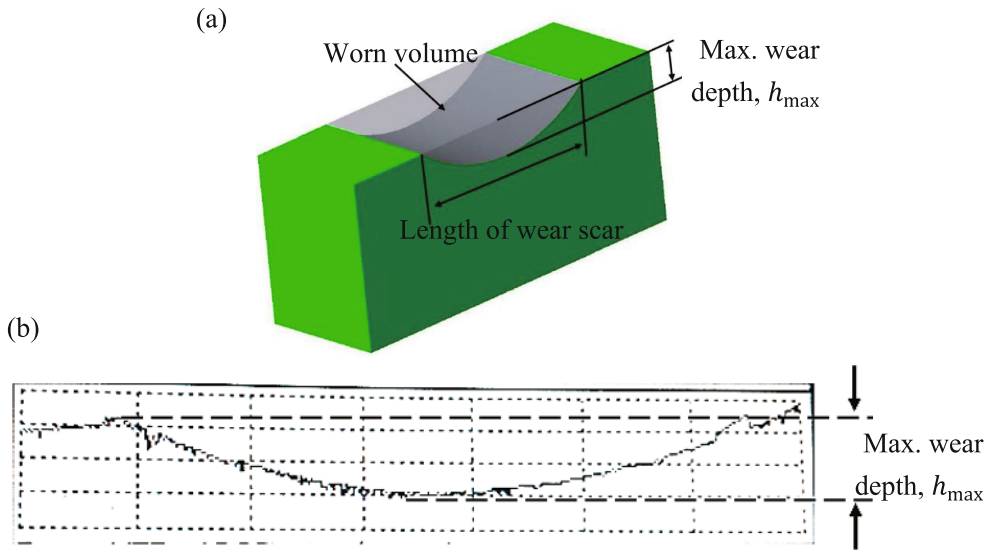

Fig. 2 (a) 3D schematic illustration of the worn volume and (b) typical wear profile of the test specimen due to sliding in BOR configuration obtained from the surface roughness tester.

Table 3 Average COF and k values for four cases of different applied loads. The standard deviations were calculated from three test attempts as per ASTM G77 standard.

Case	Applied load (N)	Average COF	Wear coefficient k (10^{-5} mm^3/(N·m))					
			1 km	2 km	3 km	4 km	5 km	6 km
1	15	0.62 ± 0.05	2.45 ± 0.25	2.21 ± 0.23	1.77 ± 0.19	1.67 ± 0.15	1.60 ± 0.19	1.57 ± 0.19
2	30	0.56 ± 0.05	1.63 ± 0.16	1.25 ± 0.14	1.06 ± 0.13	1.05 ± 0.12	1.05 ± 0.13	1.04 ± 0.13
3	45	0.55 ± 0.04	1.77 ± 0.17	1.53 ± 0.15	1.47 ± 0.16	1.42 ± 0.16	1.42 ± 0.15	1.41 ± 0.16
4	60	0.51 ± 0.04	1.74 ± 0.18	1.37 ± 0.16	1.32 ± 0.15	1.45 ± 0.17	1.63 ± 0.17	1.81 ± 0.20

the polymer–metal contact in the BOR configuration. The aim of this modelling is to analyse the adhesive wear and to understand the effect of the geometrical change of such a configuration on the wear nature. In this model, Archard's equation (Eq. (1)) [7, 31] was used as the base equation to estimate the wear coefficient. It is worth mentioning here that Archard's equation has the capability of being localised by dividing both sides on the contact area A; hence, it can be easily used in the FE modelling (Eq. (4)).

$$h = k \cdot S \cdot P \cdot \Delta N \tag{4}$$

where h is the wear depth, k is the wear coefficient including the hardness effect (k/H), P is the normal stress, and ΔN is the update interval cycle used to accelerate the modelling.

A 2D model was developed to simulate the adhesive wear process at the contact zone between the block (specimen) and ring (counterface). Sliding contact was modelled using the adaptive meshing constraint in Abaqus standard. The contact line located between the block and the ring renders the problem ideally for 2D modelling, as shown in Fig. 3. The mesh element was a 4-node bilinear plane stress quadrilateral (CPS4) for both bodies. The element's size was reduced down to 0.1 mm at the contact surface in order to obtain a converged solution.

In this model, the centre of the ring was fixed to have no displacement and the normal force was applied to the bottom surface of the block. To model the adhesive wear process, a unique FORTRAN-UMESHMOTION subroutine was created and linked with Abaqus in association with the adaptive mesh constraint, thus the subroutine's code can control the node position at the contacting surface [12, 17]. The flowchart of the wear model is presented in Fig. 4 showing the interaction between Abaqus and the UMESHMOTION subroutine. Due to the change

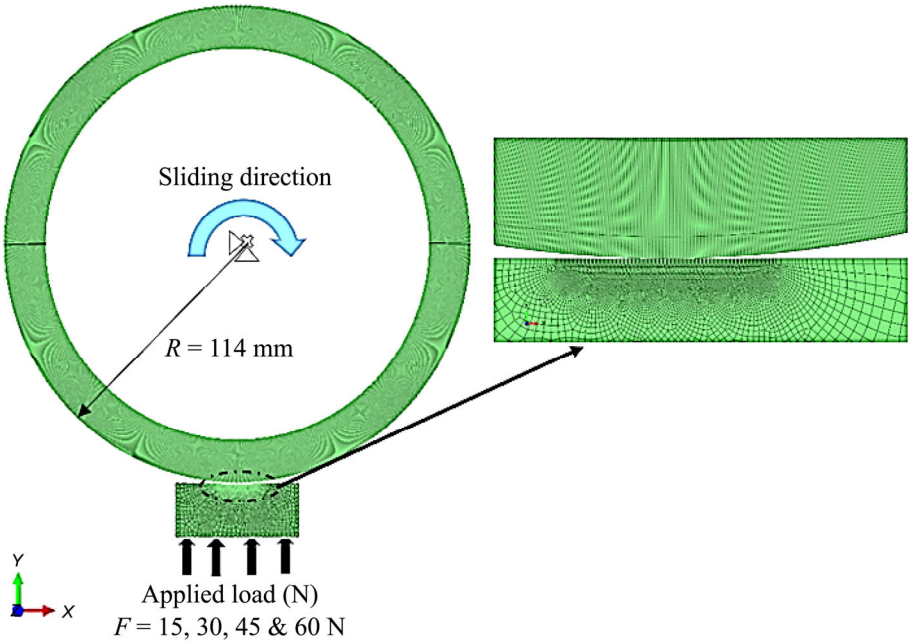

Fig. 3 Illustration of the 2D model in BOR configuration showing the FE mesh.

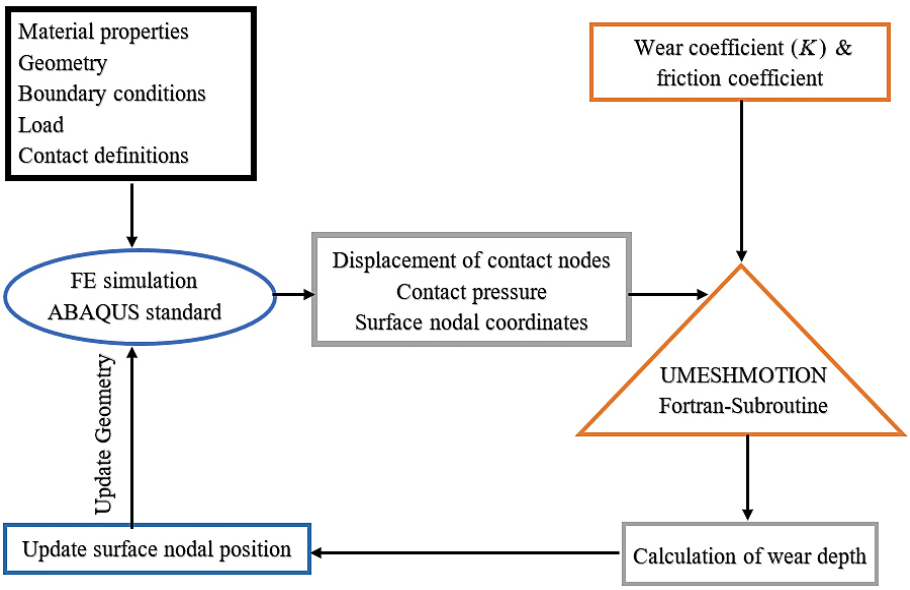

Fig. 4 Flowchart for the simulation of adhesive wear using UMESHMOTION subroutine.

in the node position, the contact profile was continuously changing and thus the relative displacement, as well as the magnitude of the contact pressure were changed for each contact node. Accordingly, new values were reported to the UMESHMOTION code and then updated for the next increment [11, 12, 32]. It should be mentioned here that the node wears once it is subjected to contact pressure only, i.e., when the node shifts to the contact interface. Adaptive mesh tools are used to improve the simulation process, as they take into account the effect of the geometrical change and the shape of wear profile during the wear process [12, 33]. The volumetric wear rate was calculated by applying $h = h_{max}$ in Eq. (2), where h_{max} is the maximum wear depth of the wear profile (Fig. 2).

To apply the Archard's equation on the contact line between the block and ring, various values of k and COF were determined through the data listed in

Table 3. As indicated by the experiments, FE modelling showed that the COF reaches its stable values after 80 sliding cycles out of the 6,000 for the entire test. Therefore, the average values of the COF were taken in the steady-state region for each case from three specimens. The k values were implemented in the model in which each 1 km of sliding distance corresponds to 1,000 sliding cycles. The current values used in developing the model are in good agreement with those reported in the literature. For instance, the k value was reported in the 0.9×10^{-5}–3.6×10^{-5} mm^3/(N·m) range by Yousif et al. [34] for epoxy composites reinforced with abrasive particles. Furthermore, Shalwan and Yousif [35] reported the k values for epoxy from 1.45×10^{-5} to 3.1×10^{-5} mm^3/(N·m) under several loads in the 20–60 N range. Thus, it is reasonable to use the k values (Table 3) in modelling the wear behaviour of the tested specimens under different conditions.

The mechanical properties of the ring are: density of 8,000 kg/m^3, stiffness of 200 GPa, yield strength of 620 MPa, and Poisson's ratio of 0.275 [36]. The stainless–steel counterpart was assumed to be a rigid counterface for the epoxy specimens. From experiments, it was noticed that the epoxy specimens sacrifice for the tribosystem in which the material transfer from the epoxy to the stainless steel counterface. The recrystallization temperature of AISI 304 is above 900 °C [37], while the glass transition temperature of epoxy is 100 °C [38]. Under the current experimental circumstances, it cannot be possible for the diffusion process to take place between the two counterparts in terms of temperature effect, and thus no material will transfer from both sides on the atomic level. It was confirmed in a previous study by the same research group [23] that the epoxy melts during the BOR test and signs of transfer films were observed on the steel ring. The effect of temperature on the wear behaviour of epoxy composites was thoroughly discussed in Ref. [23] and will not be repeated here. The influence of steel counterpart on the entire tribosystem is considered negligeable in this study. In terms of mechanical properties, the AISI 304 possesses high mechanical properties compared to the tested epoxy specimens used in this study. For instance, the stiffness of AISI 304 stainless steel is higher than the highest stiffness value of epoxy by about 170 times. Moreover, polymers may lose their stiffness quickly with the increase of the interface temperature as compared to metals.

To simplify the wear simulation, wear was only implemented in the epoxy specimens (block), as it is the softer material. It is worth noting that a high value of ΔN (Eq. (4)) gives erratic results; however, low value increased the computational time. Therefore, to adopt an appropriate ΔN value, many attempts were made for each case separately. The ΔN factor was optimised in such a way that the total wear volume in the model is matched with experimental findings.

In a BOR configuration, the highest contact pressure is at the beginning of the wear process. This is accompanied by a rapid change in the maximum wear depth. This behaviour was experimentally reported and defined as the running-in stage [39, 40]. By calling Table 3, it is apparent that k values dramatically changed in the first 3 km of sliding distance. However, with the increase of sliding distance, the contact area becomes larger as compared to the beginning of the process, where it achieves a steady state as presented. Based on this behaviour, firstly, a small value of ΔN equals to 100 was assigned for the running-in stage. Secondly, ΔN increased to 1,000 for the steady-state region. The FE modelling validated by the experiments was verified by using the chosen values of ΔN and the model was accurate enough.

3 Results and discussion

3.1 Model validation

This section describes the ability of the developed model implemented by the UMESHMOTOIN subroutine to simulate adhesive wear mechanism of polymer–metal contact. The model was designed to be quite similar to the vitro of BOR tribometer. Therefore, the objective of this step is to study the developed model's capability to analyse the wear process under specific conditions. Figure 5 shows a comparison between the simulated and experimental results. In all different experimental conditions, a good correlation was noted with the model outputs. Figures 5(a) and 5(b) represent the simulated and experimental results of the wear

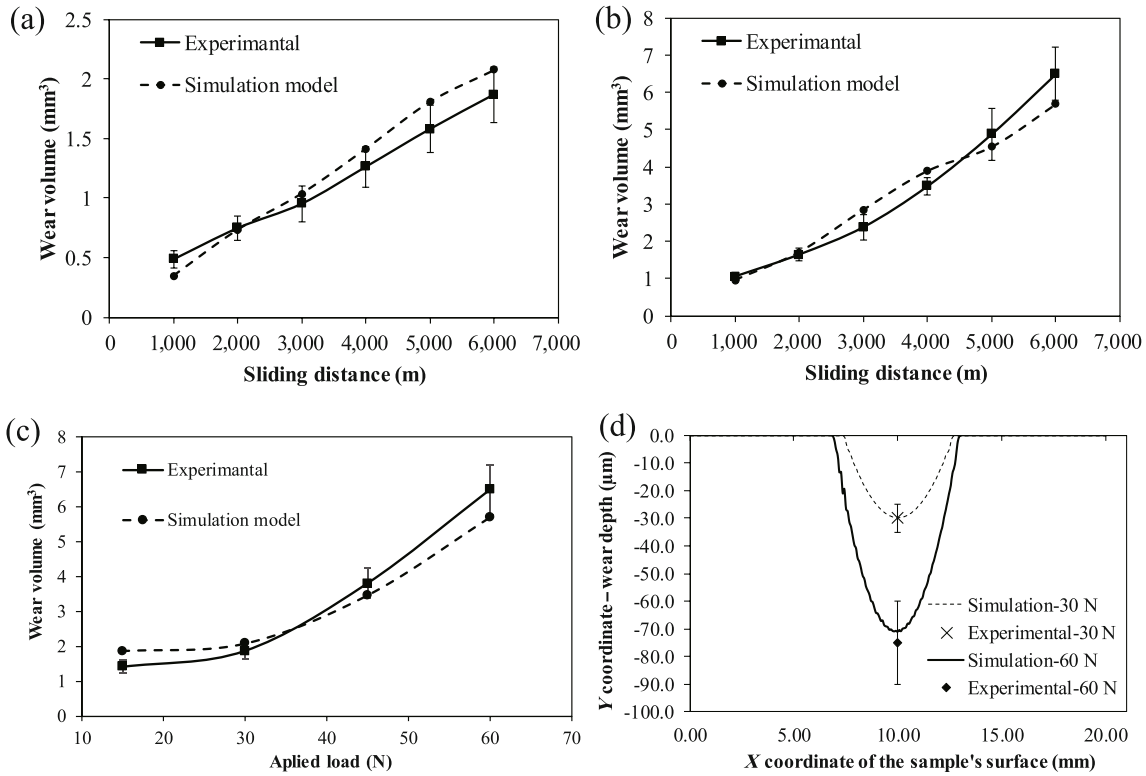

Fig. 5 Comparison between numerical and experimental investigations. (a) and (b) Wear volume versus sliding distance at 30 and 60 N, respectively; (c) wear volume at different applied loads, and (d) the simulated wear profiles and the maximum wear depths obtained from experiments at applied loads of 30 and 60 N.

volume versus sliding distance of the epoxy at a mild load of 30 N and a high load of 60 N, respectively. Figure 5(c) shows the experimental and simulated results of the wear volume under different applied loads. Excellent correlation was noted at a lower sliding distance (Fig. 5(a)) and at lower applied loads (Fig. 5(c)). Generally, there is an increase in the error with more sliding distance and applied load.

The effect of frictional heat generation on the wear calculations was not considered in the wear model. Thus, any changes in the material properties, such as strength, stiffness and hardness, were not taken into account due to a rise in the heat. Similar consideration was taken by Dos Reis [41] who attributed the change in mechanical properties to the sensitivity of the resin properties at elevated temperature. The COF may be partially responsible for the difference between the simulated and experimental results. The COF was taken as an average value despite the ± 5% fluctuation during the experimental testing. Other factors, such as the transfer film effect, wear debris, and surface roughness, which increase the challenges of simulating the wear phenomenon were also not taken into consideration. During the experiments, there was uneven material loss along the ring's axis. Therefore, the average h_{max} along the axis was taken into account, because it is considered a random phenomenon and was used to compare with the simulation results. Similar technique was reported in Refs. [42, 43]. Overall, the error percentages of the simulation results did not exceed ± 15%, which is reasonable, especially when compared with the error ranges in tribology experiments [2, 16]. The maximum wear depth (Fig. 2(b)) was estimated experimentally by using the surface roughness tester and these results were compared with the simulation results presented in Fig. 5(d) for the epoxy at 30 and 60 N applied loads. Clearly, the maximum wear depth of the simulated wear profile is located in the range of the experimental cases, as listed in Table 4.

3.2 Geometrical effect

One of the main study objectives of the wear simulation in the BOR configuration was to analyse

Table 4 Simulated and experimental values of the h_{max} for all studied cases.

Case	Applied load (N)	h_{max} (μm) from the simulation	h_{max} (μm) from the experiments
1	15	28.93	25 ± 5
2	30	29.66	30 ± 5
3	45	46.15	45 ± 10
4	60	70.85	75 ± 13

the effect of geometrical changes on the wear process and the nature of the contact itself. Therefore, the effect of the progressive change in the geometry of the wear specimen was analysed. All simulations were run similarly to the experiments for 6 km sliding distance, in an attempt to calculate the wear volume. The *PV* factor was altered, relying on different load levels, 15, 30, 45, and 60 N, and a speed of 2 m/s was used. Different loads correspond to the contact pressures ranging from 0.35 to 0.53 MPa at the steady-state region were applied.

In a configuration system like a BOR tribometer, the progressive change in the geometry is supposed to have a high effect on the resulting wear process. The fast change in the wear profile may generate concomitant stress concentrations due to geometrical changes of the specimen. Figure 6(a) shows the contact area plotted against the sliding distance under different applied loads for epoxy. Obviously, there is an increase in the contact area with increased sliding distance due to the material removal process. Since the contact area increases with sliding distance, the applied load will be distributed over an increasingly larger contact area, thus lowering the contact pressure, as shown in Fig. 6(b).

It can be seen in Fig. 6 that there is a rapid change in the contact area and contact pressure within the first 1,000 m of sliding distance. This rapid change is attributed to the load/contact area ratio being very high at the beginning of the wear process, i.e., the running-in stage [39, 40]. For instance, at 30 N, 63% reduction in the contact pressure was recorded, while the contact area increased by 288% after 1,000 m. Beyond that, it seems that the wear reaches a relatively steady state, indicated by the slow increase in the contact area and a decrease in the contact pressure.

Stress concentration is a crucial parameter that affects the wear mechanism of materials [44]. Concentrated stress promotes crack propagation and the failure mechanism on the worn surface of the wear specimen. In the current configuration, even though the normal pressure decreases with an increase in the sliding distance, the maximum wear depth (h_{max}) increases consequently. Figure 7 shows the values of the Von Mises stress, shear stress, and stress concentration versus the contact length. Simulation results show that there is a significant increase in the stress values with the increase of h_{max}. Figure 7(a) displays the contours of Von Mises and shear stresses after a sliding distance of 3 and 6 km. The more interesting point is the effect of the sliding direction. The stress is highly concentrated at the starting edge, heading towards the end edge, as described by arrows. This difference stems from the high friction at the starting edge. Observation of stress concentration at the edges of the wear profiles was reported as fretting wear mechanism [19–21]. However, due the cycling mechanism of the sliding contact of fretting wear, the stress concentrations were almost symmetric at both edges of the wear profiles. Experimentally, the explanation of this observation is attributed to the

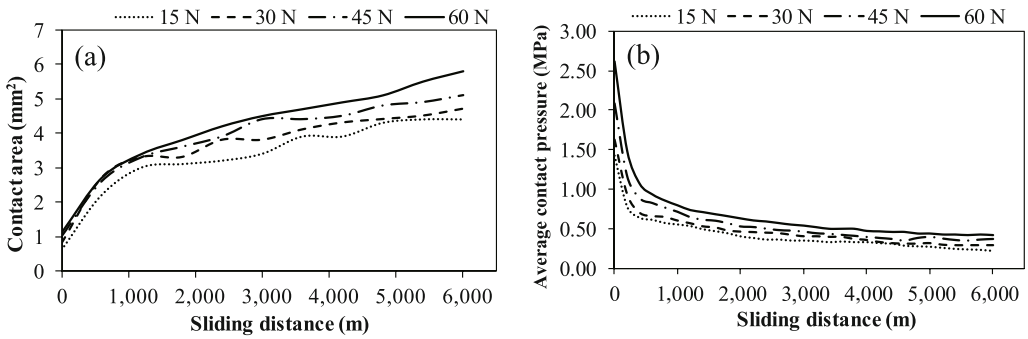

Fig. 6 Effect of various applied loads for epoxy on (a) change of contact area and (b) change of average contact pressure, for 6 km of sliding distance.

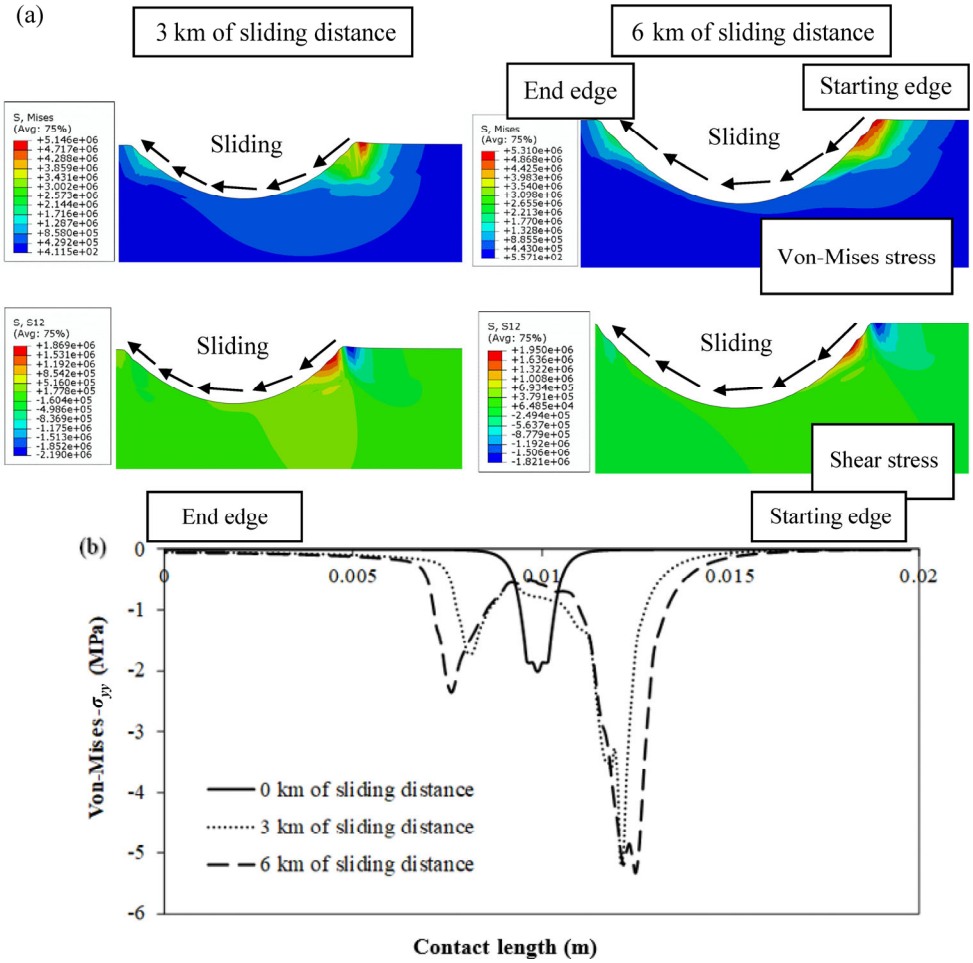

Fig. 7 (a) Stress contours after 3 and 6 km of sliding distances and (b) stress distribution profile represented by Von Mises (σ_{yy}) versus contact position.

high interlocks between the asperities of the wear specimen and the steel ring at this edge [5, 39, 45, 46]. In the current study, Fig. 7(b) shows the stress distribution profile represented by Von-Mises stress contours, for initial, middle, and final sliding distances (0, 3, and 6 km). It is worth noting that the plotted graphs represent the surface nodes on the block (wear specimen) in the contact region. At the middle region, where h_{max} exists, the contact pressure is decreased with the increase of sliding distance, which is consistent with the general analysis of geometrical change of the wear specimen (Fig. 6).

At the edges of the stress distribution profile, extremity in the stress values was observed. This was due to the change of the wear profile. Typically, on both sides and due to their similarity, the increased stress value could be attributed to the change in the specimen's geometry. However, a greater increase was observed in the stress values at the starting edge, as compared with the end edge. For instance, the 6 km sliding distance showed higher stress values by about 940% and 350% at the starting edge and the end edge, respectively, as compared to the stress value for the same distance at the middle region. Similar stress contours were observed at both edges for all used applied loads. This finding highlights the effect of stress concentration on the wear mechanism, which needs to be considered during the analysis stage. This complies with the basic principle of design, which always seeks to find the most effective parameters, i.e., stress concentrations.

Figure 8 shows the effect of various applied loads, taken at the node that corresponds to the h_{max}, on the mechanical stresses and after 6 km. The stress values increased significantly after 30 N, evidenced by the increase in the wear coefficient value, as reported

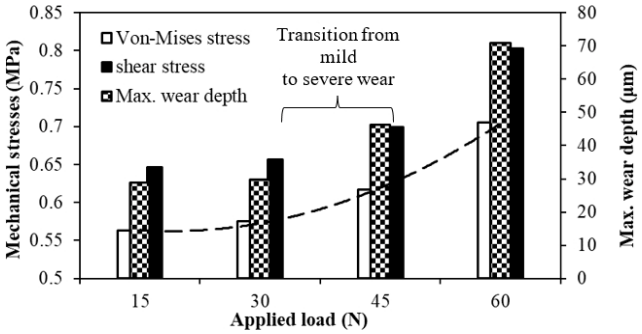

Fig. 8 Influence of applied load and the maximum wear depth on the mechanical stress including Von Mises stress and shear stress at the node of the maximum wear depth (original contact point).

in Table 3. Therefore, it was considered that the mild-to-severe wear transition took place when the applied load exceeded 30 N. Similar findings was observed by the authors in a previous studies [23, 24]. However, it can be noticed that the average mechanical stresses (Von-mises and shear stresses) increased by only around 25% at 60 N as compared to that in the mild region, i.e., 30 N (100% increase in the applied load) (see Fig. 8). This is evidence that the stress concentration exhibited more effect on the wear mechanism of wear samples as compared to the effect of the applied loads shown in Fig. 7.

3.3 SEM analysis of the worn surfaces

Based on the simulation results, two areas were chosen on the worn surfaces of the wear specimens as demonstrated in Fig. 9. The first area (Zone a), the largest area of the wear profile, is known as the normal zone, which is under average contact stresses. The second area (Zone b), known as the critical zone, is where the stress concentration is the highest. Accordingly, SEM micrographs were taken for these zones for all wear specimens.

Figures 10 and 11 show the SEM micrographs of the wear specimens, under different applied loads,

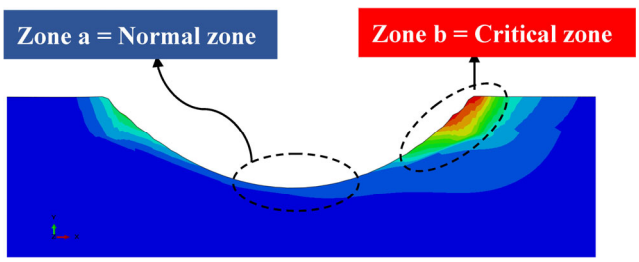

Fig. 9 Demonstration of the two zones (normal and critical zones).

after 6 km of sliding distance. There is an observable difference between the features in normal and critical zones. At the normal zone (Fig. 10), a remarkable difference after 30 N of applied load was observed when the wear transmitted from the mild region to the severe region. In the mild region of 15 and 30 N, it can be noted that the worn surfaces exposed microcracks and fragmentation failures as shown in Figs. 10(a) and 10(b), respectively. However, extreme

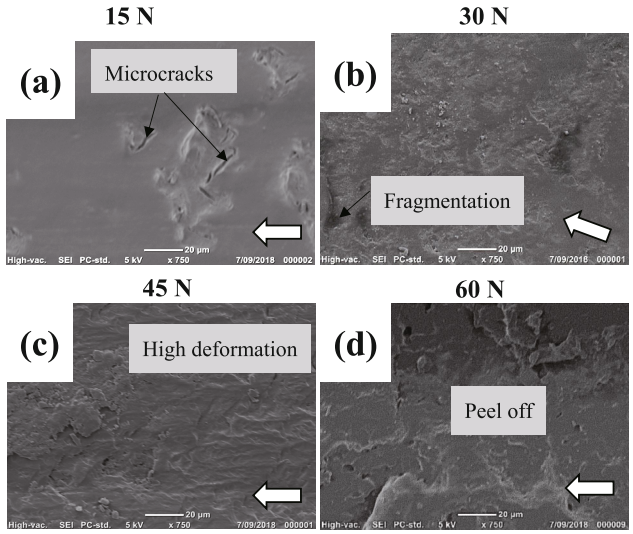

Fig. 10 SEM micrographs at normal zone of the worn surfaces of wear specimens, at different applied loads: (a) 15, (b) 30, (c) 45, and (d) 60 N. The arrows on the bottom-right corner indicate the sliding direction of the ring.

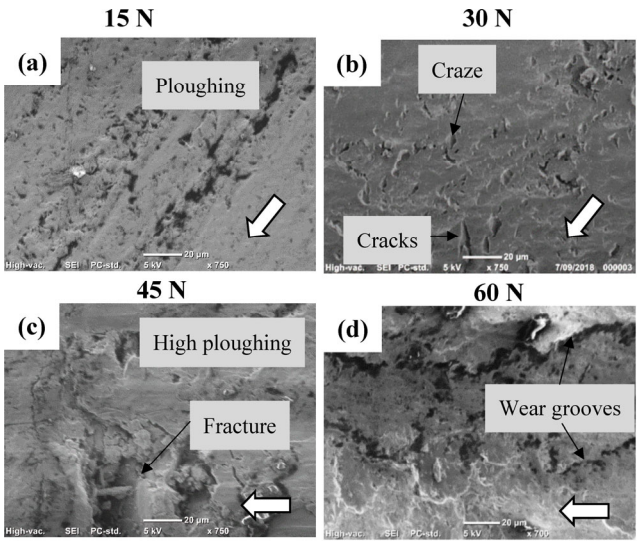

Fig. 11 SEM micrographs at the critical zone of the worn surfaces of wear specimens, at different applied loads: (a) 15, (b) 30, (c) 45, and (d) 60 N. The arrows on the bottom-right corner indicate the sliding direction of the ring.

failure signs were noted in the severe wear region in which the applied loads ranged between 45 and 60 N as shown in Figs. 10(c) and 10(d), respectively. These signs were in the form of high deformation and peeling off. The normal zone analysis was performed in a previous work done by the same research group [23].

Clear signs of severe wear features, manifested by ploughing, craze, cracks, fracturs, and wear grooves were observed in the critical zone under different applied loads as shown in Fig. 11. Interestingly, these results are in harmony with the simulation findings, as discussed in Section 3.2. It is essentially to mention that the critical zone is subjected to a high stress rates, reaching up to 10 times more than that at the normal zone. These observations can explain the experimental findings presented in Fig. 12. At 30 N of applied load, the lowest value of the wear rate was recorded, even when it was compared to an applied load of 15 N. A brief explanation of this behaviour could be as follows: First, the specimen under 30 N seems to experience enough heat that can form a viscoelastic layer and thus protects the worn surface from further mass loss [23, 47]. This thin layer inhibits the initiation of a brittle cracking scenario in the matrix under the fatigue loads as was noticed in the case under 15 N. Similar behaviour was reported by Yousif and El-Tayeb [48] who studied the effect of the applied load (5, 10, 15, and 20 N) on the wear rate of glass fibres reinforced polyester under abrasive wear conditions. It was noticed that the increase of the applied load reduced the wear rate. Similar trend was also reported by Chand and Dwivedi [49] on sisal fibre-reinforced epoxy composites. However, for applied loads higher than 30 N, there is a much increase in the thermo-mechanical stresses, which result in further material removal, in the form of high ploughing, and severe wear grooves [23, 35, 50].

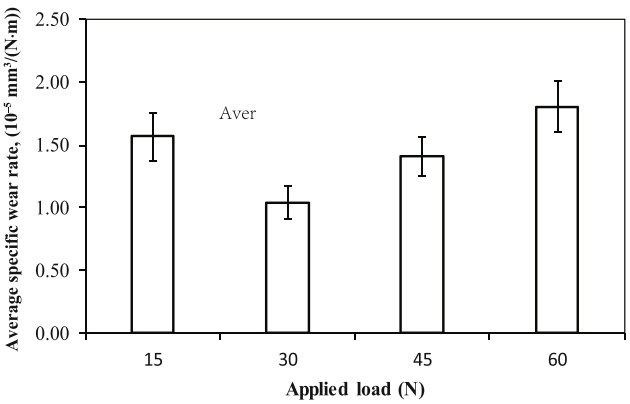

Fig. 12 Effect of applied load on the specific wear rate of epoxy after 6 km, i.e. steady state region, of sliding distance.

The analysis made in this study showed that the stress distribution profile has a consistent pattern for all applied cases. The stress profiles subtracted from the wear modelling analysis provide a better understanding of the wear phenomenon on the BOR configuration. Similar circumferential contacts in real tribo-component applications, such as bearings, bushings, camshafts, and so on can also be described using such approach. Knowing that the wear coefficient (k) is almost unchanged in the steady-state region of the wear process, the developed model can accordingly be useful to predict the wear behaviour of the tribo-components and estimate their service lives.

4 Conclusions

In this paper, a two-dimensions (2D) model of a ball-on-ring (BOR) tribometer was developed to analyse the adhesive wear mechanism in a polymer–metal contact. The simulation model was based on the Archard's wear equation implemented by a Fortran-UMESHMOTION subroutine linked with Abaqus, with an adaptive meshing tool. Based on these results, the following conclusions were drawn:

1) This model was used to analyse the impact of geometrical change on the wear nature of BOR configuration. The wear model displayed high reliability to simulate the wear volume at mild and severe regions, showing the transition point between both regions. The model was in good agreement with the experimental results.

2) Generally, it was understood that the contact pressure decreases with the increase of the wear depth due to the increase in the contact area of the worn surface. However, and for all the studied cases, the critical wear zone appeared, representing the main interesting finding in this study.

3) The critical zone is characterized by high concentration of stresses reaching up to 10 times of the normal stress values. The stress concentration proportionally increases with the increase of the wear

depth. Based on this, the wear profile was divided into two specific areas: the normal area, which represents the majority of the worn surface subjected to the average stress and the critical area in which the stresses are highly concentrated at the starting edge of the wear profile.

4) scanning electron microscope (SEM) was used to support the stress analysis of the wear profiles for all studied cases. It was noticed that the worn surfaces of the wear specimens at the critical zone suffered from high damage compared with that at the normal zone. Therefore, this study has defined the critical zone of BOR configuration which has to be investigated in accordance with the basic concept of the design.

Acknowledgements

The first author is thankful for the Ph.D. scholarship sponsored by Tafila Technical University, Tafila, Jordan. The assistance from technicians and colleagues in the Centre of Future Materials (CFM) is also acknowledged.

Declaration of competing interest

The authors have no competing interests to declare that are relevant to the content of this article.

References

[1] Friedrich, K. Polymer composites for tribological applications. *Adv Ind Eng Polym Res* **1**: 3–39 (2018)

[2] Hegadekatte V, Huber N, Kraft O. Finite element based simulation of dry sliding wear. *Model Simul Mater Sci Eng* **13**: 57 (2004)

[3] Hegadekatte V, Hilgert J, Kraft O, Huber N. Multi time scale simulations for wear prediction in micro-gears. *Wear* **268**: 316–324 (2010)

[4] Bose K K, Ramkumar P. Finite element method based sliding wear prediction of steel-on-steel contacts using extrapolation techniques. *Proc Inst Mech Eng Part J J Eng Tribol* **233**: 1446–1463 (2019)

[5] Nirmal U, Hashim J, Megat Ahmad M M H. A review on tribological performance of natural fibre polymeric composites. *Tribol Int* **83**: 77–104 (2015)

[6] Meng H C, Ludema K C. Wear models and predictive equations: Their form and content. *Wear* **181:** 443–457 (1995)

[7] Archard J F. Wear theory and mechanisms. In *Wear Control Handbook*. Peterson M B, Winer W O, Ed. New York: ASME, 1980, 35–80.

[8] Sarkar A D. *Friction and Wear*. London (UK): Elsevier, 1982.

[9] Sarkar A D. *Friction and Wear*. New York (USA): CRC press, 1980.

[10] Liu R, Li D Y. Modification of archard's equation by taking account of elastic/pseudoelastic properties of materials. *Wear* **251**: 956–964 (2001)

[11] Bortoleto E M, Rovani A C, Seriacopi V, Profito F J, Zachariadis D C, Machado I F, Sinatora A, de Souza R M. Experimental and numerical analysis of dry contact in the pin on disc test. *Wear* **301**: 19–26 (2013)

[12] Fallahnezhad K, Oskouei R H, Badnava H, Taylor M. An adaptive finite element simulation of fretting wear damage at the head-neck taper junction of total hip replacement: The role of taper angle mismatch. *J Mech Behav Biomed Mater* **75**: 58–67 (2017)

[13] Hegadekatte V, Kurzenhäuser S, Huber N, Kraft O A. Predictive modeling scheme for wear in tribometers. *Tribol Int* **41**: 1020–1031 (2008)

[14] Martinez F J, Canales M, Izquierdo S, Jimenez M A, Martinez M A. Finite element implementation and validation of wear modelling in sliding polymer–metal contacts. *Wear* **284**: 52–64 (2012)

[15] Hegadekatte V, Huber N, Kraft O. Modeling and simulation of wear in a pin on disc tribometer. *Tribol Lett* **24**: 51 (2006)

[16] Arjmandi M, Ramezani M, Giordano M, Schmid S. Finite

element modelling of sliding wear in three-dimensional woven textiles. *Tribol Int* **115**: 452–460 (2017)

[17] Fallahnezhad K, Oskouei R H, Taylor M. Development of a fretting corrosion model for metallic interfaces using adaptive finite element analysis. *Finite Elem Anal Des* **148**: 38–47 (2018)

[18] Benabdallah H, Olender D. Finite element simulation of the wear of polyoxymethylene in pin-on-disc configuration. *Wear* **261**: 1213–1224 (2006)

[19] Yue T, Abdel Wahab M. A numerical study on the effect of debris layer on fretting wear. *Materials (Basel)* **9**: 597 (2016)

[20] Fallahnezhad K, Oskouei R H, Badnava H, Taylor M. An adaptive finite element simulation of fretting wear damage at the head-neck taper junction of total hip replacement: The role of taper angle mismatch. *J Mech Behav Biomed Mater* **75**: 58–67 (2017)

[21] English R, Ashkanfar A, Rothwell G. A computational approach to fretting wear prediction at the head–stem taper junction of total hip replacements. *Wear* **338–339**: 210–220 (2015)

[22] Prasad V, Suresh D, Joseph M A, Sekar K, Ali M. Development of flax fibre reinforced epoxy composite with nano TiO_2 addition into matrix to enhance mechanical properties. *Mater Today Proc* **5**: 11569–11575 (2018)

[23] Eayal Awwad K Y, Yousif B F, Fallahnezhad K, Saleh K, Zeng X. Influence of graphene nanoplatelets on mechanical properties and adhesive wear performance of epoxy-based composites. *Friction* **9**(4): 856–875 (2021)

[24] Awwad K E, Yousif B, Mostafa A, Alajarmeh O, Zeng X. Tribological and mechanical performances of newly developed eco-epoxy composites incorporating flax fibres and graphene nanoplatelets. *J Reinf Plast Compos* 073168442211434 (2022)

[25] Briscoe B J, Sinha S K. Tribological applications of polymers and their composites—Past, present and future prospects. In *Tribology of Polymeric Nanocomposites*. Briscoe B J, Ed. Amsterdam (Holland): Elsevier, 2013: 1–22.

[26] US-ASTM. ASTM D974-2014 Standard test method for tensile properties of plastics. ASTM, 2014.

[27] US-ASTM. ASTM D2240-2005 Standard test method for t rubber property–durometer hardness 1. ASTM, 2005.

[28] US-ASTM. ASTM G77-2017 Standard test method for ranking resistance of materials to sliding wear using block-on-ring wear test. ASTM, 2017.

[29] Volume of a partial right cylinder calculator—High accuracy calculation. https://www.mathopenref.com/cylindervolpartial.html, 2023.

[30] Archard J F. Contact and rubbing of flat surfaces. *J Appl Phys* **24**: 981–988 (1953)

[31] Chattopadhyay R. *Green Tribology, Green Surface Engineering, and Global Warming*. Ohio (USA): ASM International, 2014.

[32] Khader I, Renz A, Kailer A. A wear model for silicon nitride in dry sliding contact against a nickel-base alloy. *Wear* **376**: 352–362 (2017)

[33] Bitter T, Khan I, Marriott T, Lovelady E, Verdonschot N, Janssen D. Finite element wear prediction using adaptive meshing at the modular taper interface of hip implants. *J Mech Behav Biomed Mater* **77**: 616–623 (2018)

[34] Yousif B F, Nirmal U, Wong K J. Three-body abrasion on wear and frictional performance of treated betelnut fibre reinforced epoxy (t-bfre) composite. *Mater Des* **31**: 4514–4521 (2010)

[35] Shalwan A, Yousif B F. Influence of date palm fibre and graphite filler on mechanical and wear characteristics of epoxy composites. *Mater Des* **59**: 264–273 (2014)

[36] Stainless Steel-Grade 304, Atlas Steel Australia, 2019: 1–3.

[37] Valentini L, Di Schino A, Kenny J M, Gerbig Y, Haefke H. Influence of grain size and film composition on wear resistance of ultra fine grained AISI 304 stainless steel coated with amorphous carbon films. *Wear* **253**: 458–464 (2002)

[38] Li P, Zheng Y, Li M, Shi T, Li D, Zhang A. Enhanced toughness and glass transition temperature of epoxy nanocomposites filled with solvent-free liquid-like nanocrystal-functionalized graphene oxide. *Mater Des* **89**: 653–659 (2016)

[39] Nirmal U, Hashim J, Low K O. Adhesive wear and frictional performance of bamboo fibres reinforced epoxy composite. *Tribol Int* **47**: 122–133 (2012)

[40] Nirmal U, Yousif B F, Rilling D, Brevern P V. Effect of betelnut fibres treatment and contact conditions on adhesive wear and frictional performance of polyester composites. *Wear* **268**: 1354–1370 (2010)

[41] Dos Reis J M L. Effect of temperature on the mechanical properties of polymer mortars. *Mater Res* **15**: 645–649 (2012)

[42] Done V, Kesavan D, Krishna R M, Chaise T, Nelias D. Semi analytical fretting wear simulation including wear debris. *Tribol Int* **109**: 1–9 (2017)

[43] Warmuth A R, Pearson S R, Shipway P H, Sun W. The effect of contact geometry on fretting wear rates and mechanisms for a high strengthsteel. *Wear* **301**: 491–500 (2013)

[44] Yıldırım Ç V, Sarıkaya M, Kıvak T, Şirin Ş. The effect of addition of hbn nanoparticles to nanofluid-mql on tool wear patterns, tool life, roughness and temperature in turning of Ni-based inconel 625. *Tribol Int* **134**: 443–456 (2019)

[45] Bajpai P K, Singh I, Madaan J. Tribological behavior of natural fiber reinforced PLA composites. *Wear* **297**: 829–840 (2013)

[46] Mostafa A O. Mechanical properties and wear behavior of aluminum grain refined by Ti and Ti+B. *Int J Surf Eng Interdiscip Mater Sci* **7**: 1–19 (2019)

[47] Akpan E I, Wetzel B, Friedrich K. A fully biobased tribology material based on acrylic resin and short wood fibres. *Tribol Int* **120**: 381–390 (2018)

[48] Yousif B F, El-Tayeb N S M. Wear characteristics of thermoset composite under high stress three-body abrasive. *Tribol Int* **43**: 2365–2371 (2010)

[49] Chand N, Dwivedi U K. Influence of fiber orientation on high stress wear behavior of sisal fiber-reinforced epoxy composites. *Polym Compos* **28**: 437–441 (2007)

[50] Omrani E, Menezes P L, Rohatgi P K. State of the art on tribological behavior of polymer matrix composites reinforced with natural fibers in the green materials world. *Eng Sci Technol an Int J* **19**: 717–736 (2016)

K. Y. Eayal AWWAD. He has received his M.Sc. degree in mechanical engineering from the University of Jordan, Amman, Jordan, in 2015. After that, he received his Ph.D. degree from the University of Southern Queensland (USQ), Toowoomba, Queensland, Australia, in 2020. He has joined the Mechanical Engineering Department as an assistant professor at Tafila Technical University (TTU), Tafila, Jordan. His research areas cover solid lubricants, tribology, and wear mechanisms of nanocomposites and polymeric composites, and natural fiber polymeric composites. In addition, his research interest includes grain refinement in alloys, micro-metal alloys, and severe plastic deformation (SPD).